Pharm Res (2012) 29:2860–2873
DOI 10.1007/s11095-012-0792-7

RESEARCH PAPER

Physiologically Based Modeling of Pravastatin Transporter-Mediated Hepatobiliary Disposition and Drug-Drug Interactions

Manthena V. S. Varma • Yurong Lai • Bo Feng • John Litchfield • Theunis C. Goosen • Arthur Bergman

Received: 11 March 2012 / Accepted: 16 May 2012 / Published online: 26 May 2012

ABSTRACT

Purpose To develop physiologically based pharmacokinetic (PBPK) model to predict the pharmacokinetics and drug-drug interactions (DDI) of pravastatin, using the *in vitro* transport parameters.

Methods *In vitro* hepatic sinusoidal active uptake, passive diffusion and canalicular efflux intrinsic clearance values were determined using sandwich-culture human hepatocytes (SCHH) model. PBPK modeling and simulations were implemented in Simcyp (Sheffield, UK). DDI with OATP1B1 inhibitors, cyclosporine, gemfibrozil and rifampin, was also simulated using inhibition constant (Ki) values.

Results SCHH studies suggested active uptake, passive diffusion and efflux intrinsic clearance values of 1.9, 0.5 and 1.2 μL/min/10^6cells, respectively, for pravastatin. PBPK model developed, using transport kinetics and scaling factors, adequately described pravastatin oral plasma concentration-time profiles at different doses (within 20% error). Model based prediction of DDIs with gemfibrozil and rifampin was similar to that observed. However, pravastatin-cyclosporine DDI was underpredicted (AUC ratio 4.4 Vs ~10). Static (R-value) model predicted higher magnitude of DDI compared to the AUC ratio predicted by the PBPK modeling.

Conclusions PBPK model of pravastatin, based on *in vitro* transport parameters and scaling factors, was developed. The approach described can be used to predict the pharmacokinetics and DDIs associated with hepatic uptake transporters.

M. V. S. Varma (✉) • Y. Lai • B. Feng • J. Litchfield • T. C. Goosen
Pharmacokinetcis, Dynamics and Metabolism, Pfizer Inc.
Groton, Connecticut, USA
e-mail: manthena.v.varma@pfizer.com

A. Bergman
Clincial Pharmacology, Pfizer Inc.
Groton, Connecticut, USA

KEY WORDS drug-drug interaction · OATP1B1 · physiologically based pharmacokinetic (PBPK) model · pravastatin · transporters

ABBREVIATIONS

AUC	area under the plasma concentration-time curve
BCRP	breast cancer resistance protein
Cmax	maximum plasma concentration
DDI	drug-drug interaction
Fa	fraction absorbed
fu	fraction unbound
fu_{inc}	fraction unbound in the incubations
$I_{in,max}$	maximum inhibitor concentration at the inlet to the liver
Ki	inhibition constant
MRP	multidrug resistance-associated protein
OATP	organic anion transporting polypeptide
PBPK	physiologically based pharmacokinetic
PPE	percentage prediction error
SCHH	sandwich cultured human hepatocyte
SF	scaling factor

INTRODUCTION

The relationship between physiological parameters and the body size or body weight lead to the wide application of allometry to predict human pharmacokinetics utilizing the preclinical animal data (1,2). However, due to noted interspecies differences, especially in metabolizing enzymes and drug transporters, many different approaches have been proposed over the years to obtain improved predictions. Unlike allometry and other empirical pharmacokinetic models, physiologically based pharmacokinetic (PBPK)

models provide mechanistic time-based profiles by integrating drug-dependent and human physiological-dependent parameters, in the process of predicting human pharmacokinetics (3,4). In addition to allowing for human pharmacokinetics predictions at the discovery stage, PBPK modeling is also useful in early- and late-stage development to predict drug exposure in situations including, drug-drug interactions (DDIs), organ dysfunction, age and genetics (4–6). US FDA recommends use of PBPK models to quantitatively predict the magnitude of DDIs in various clinical situations; furthermore, this approach may offer useful alternatives to dedicated clinical studies (7).

Commercial softwares for whole body-PBPK include GastroPlus, PK-Sim, Simcyp, etc (8–10). The Simcyp population-based ADME simulator integrates interindividual variability into PBPK modeling for the prediction of drug disposition and DDIs in virtual populations. By combining information on physiology, genetic and demography/ethnicity with *in vitro* data, Simcyp performs extrapolation to *in vivo* situations and virtual populations (9).

Hepatobiliary transport significantly contributes to the disposition of a wide variety of drugs, especially the low permeable hydrophilic drugs typically categorised in biopharmaceutics drug disposition classification system (BDDCS) class III and IV (11,12). The organic anion transporting polypeptides (OATP, *SLC21A*) are sodium-independent transporters that facilitate transport of amphipathic organic compounds. In liver, OATP1B1, OATP1B3 and OATP2B1 are expressed on the sinusoidal membrane of hepatocytes and facilitate uptake of many clinically important anionic drugs, including HMG-CoA reductase inhibitors (statins) (13–16). The significance of these uptake transporters seems to be greatest for hydrophilic statins, such as pravastatin and rosuvastatin (16). Indeed, clinically relevant drug-drug interactions (DDIs) are attributed to the inhibition of statin transport mediated by members of the OATP family. For example, co-administration of cyclosporine resulted in about a 6- to 10-fold increase in the plasma levels of pravastatin and rosuvastatin, although these statins are not appreciably metabolized in humans (16). Furthermore, polymorphisms of *SLCO1B1* (encoding OATP1B1) may lead to low transporter activity and may decrease the cholesterol lowering effect of statins (eg. Pravastatin (17)), presumably due to decreased hepatic drug exposure and concomitant increase in plasma concentrations; which could increase relative peripheral tissue exposure and the risk of muscle toxicity (18–20).

Biliary and renal clearance are the main elimination pathways of pravastatin from the systemic circulation, with each pathway contributing to roughly half of the total clearance (16,21). The hepatic uptake of pravastatin is mainly mediated by OATP1B1, and its biliary excretion is predominantly mediated by multidrug resistance-associated protein 2 (MRP2) (16). The hepatobiliary disposition is primarily defined by the sinusoidal active uptake, sinusoidal passive diffusion and the canalicular efflux kinetics (22,23). While, many *in vitro* and *in situ* tools have been established to estimate the transport kinetics and to understand the hepatobiliary disposition of drugs, the applicability of the data to predict human biliary disposition is not well established (24). Due to polarisation of the hepatocytes, *in vitro* sandwich cultured human hepatocyte (SCHH) model provides a better tool to estimate the transporter kinetics, while keeping intact the physiological features of the hepatocytes (22,25–27). Recently whole body-PBPK models integrating *in vitro* data from suspension hepatocytes or SCCH studies has been reported, to simulate pharmacokinetics of pravastatin and other OATP substrates (22,23). However, a comprehensive PBPK approach for predicting the transporter-mediated DDIs is currently lacking.

The objective of the present study is to develop a whole-body PBPK (Simcyp) model of pravastatin, utilizing the hepatobiliary transport (sinusoidal active uptake, passive diffusion and canalicular efflux) intrinsic clearance values obtained from SCHH studies. The PBPK model was used to simulate the oral pharmacokinetics; and study the effect of changes in hepatobiliary transport on the oral systemic exposure. Furthermore, pharmacokinetic models of OATP1B1 inhibitors, cyclosporine, gemfibrozil and rifampin, were established in order to predict DDIs of pravastatin induced by these drugs.

MATERIALS AND METHODS

Material

Pravastatin and rifamycin SV were purchased from Sigma (St. Louis, MO). Media for hepatocyte culture including *In Vitro*Gro-HT, *In Vitro*Gro-CP and *In Vitro*Gro-HI are purchased from Celsis *In Vitro* Technologies (Baltimore, MD). Hanks' balanced salt solution (HBSS) and Williams' medium E were purchased from Invitrogen (Carlsbad, CA). BioCoat 24-well plates and Matrigel were purchased from BD Biosciences (Bedford, MA).

Transport Studies Using Sandwich-Culture Human Hepatocyte Model

Cryopreserved human hepatocytes lots HU4168, RTM and BD109 were purchased from CellzDirect (Pittsboro, NC, USA), Celsis IVT (Baltimore, MD, USA) and BD BioSciences (Woburn, MA, USA), respectively. *In Vitro*Gro-HT (thawing), *In Vitro*Gro-CP (plating), and *In Vitro*Gro-HI (incubation) media were supplemented with Torpedo Antibiotic Mix (Celsis IVT), according to the manufacturer's instructions. Cryopreserved hepatocytes were thawed and plated as described previously (25). The hepatocyte plate-

seeding density was 0.75×10^6 cells/mL for lots BD109 and RTM and 0.85×10^6 cells/mL for lot Hu4168. Pravastatin (1 μM) was incubated in the presence or absence of rifamycin SV (100 μM) and Ca^{2+}/Mg^{2+} and the initial uptake rates were calculated from the slope between 0.5 to 1.5 min (25,26). The efflux clearance values of pravastatin were estimated, as previously described (22).

Samples were analyzed using HPLC (Hewlett Packard G1310 1100 Series) followed by MS/MS (MDS Sciex API 4000). The mobile phase used to load the column (Dash HTS Hypersil Gold 20×2.1 mm 5 μm) was 2 mM ammonium acetate in 90% methanol containing 0.027% formic acid (*v/v*); elution was performed using 2 mM ammonium acetate in 10% methanol containing 0.027% formic acid (*v/v*). The mass:charge ratio (m/z) and collision energies (eV) for pravastatin were m/z 423➔101 -40 eV.

Pharmacokinetic Modeling and Simulations

Whole-body PBPK modeling and simulations of clinical pharmacokinetics and the transporter-based drug interaction were performed using population-based ADME simulator, Simcyp (version 11.0, SimCYP Ltd, Sheffield, UK). Each simulation was performed for 50 subjects (5 trials×10 subjects). The virtual populations of healthy subjects had a body weight of 70 kg, with age ranging from 18 to 65 years, and included both sexes. Dose, dosing interval, and dosing duration of pravastatin alone or co-dosing with cyclosporine, gemfibrozil and rifampin in the simulation were similar to that used in the reported clinical studies (21,28–31).

Pravastatin PBPK Model Development

An initial model of pravastatin was build using the physicochemical properties, *in vitro* preclinical data such as human plasma unbound fraction (fu) and blood-to-plasma ratio, and *in vivo* clinical pharmacokinetic parameters such as renal clearance (Table I). Full-PBPK model using Rodger *et al.* method (32,33) considering rapid equilibrium between blood and tissues was adopted to obtain the distribution of pravastatin into all organs, except liver. Permeability-limiting distribution was considered for liver; where active uptake intrinsic clearance and passive diffusion across the sinusoidal membrane and efflux intrinsic clearance on the canalicular membrane, obtained from SCHH studies, are incorporated to capture hepatobiliary disposition. Pravastatin sinusoidal uptake is predominantly mediated by OATP1B1, thus the active hepatic uptake clearance was attributed completely to the OATP1B1-mediated transport (16). On the other hand, MRP2 was assumed to be solely responsible for pravastatin canalicular efflux (16,23). Along with the general input parameters, the transport intrinsic clearance values, obtained from the SCHH studies, were used to build the initial model. However, the plasma concentration-time profile of an intravenous dose (9.9 mg dose) was over-predicted with the initial PBPK model (Fig. 1a). Therefore, scaling factors for the OATP1B1- and MRP2-mediated transport intrinsic clearances, which were initially assumed as one, were estimated simultaneously by fitting the plasma concentration-time profile of pravastatin in humans following a single intravenous dosing of 9.9 mg to the initial model, while fixing the rest of the parameters. Absorption phase in the model was captured using first-order absorption rate kinetics (Ka= 1.25/h) and fraction absorption (Fa) of 0.47 (21), and with a lag time of 15 min post dose, for all the oral doses.

Cyclosporine, Gemfibrozil and Rifampin Models and Drug-Drug Interactions

Cyclosporine and gemfibrozil models were developed using clinical first-order absorption rate, Fa and human total clearance, with volume of distribution from PBPK model or clinical reports (Table I). On the other hand, rifampin compound file is available in the Simcyp compound library, and was directly adopted (Table I). A lag time of 15 min for absorption was applied for all the oral doses of all the three inhibitor drugs. The reported *in vitro* inhibition constant (K_i) values for cyclosporine-induced OATP1B1 inhibition range from 0.014–1.0 μM (34–38). Therefore, these values were evaluated to estimate the potential *in vivo* Ki. Cyclosporine also inhibits MRP2 with Ki value of about 1.35 μM (39), which was used to capture the change in pravastatin biliary excretion in the presence of cyclosporine. Similarly, the reported *in vitro* K_i values for gemfibrozil-induced OATP1B1 inhibition range from 2.5 to 35.8 μM (36,40–43); and were evaluated to estimate the potential *in vivo* Ki. In case of rifampin, the *in vitro* Ki values ranging between 0.41–3.1 μM (36,37,44–46), were evaluated for OATP1B1 inhibition. The simulated mean AUC values of pravastatin co-administered with perpetrator or when dosed alone were used to calculate AUC ratio.

Static (R-value) Model for Predicting Drug-Drug Interactions

The degree of inhibition of uptake via OATP1B1 and thus the magnitude of DDI is predicted by calculating the R-value (7,14,47).

$$R = 1 + \left(fu.I_{in,max}\right)/Ki \quad (1)$$

where fu represents the protein unbound fraction of the inhibitor in plasma, $I_{in,max}$ represents the maximum plasma concentration of the inhibitor at the inlet to the liver. In case of cyclosporine, whole-blood concentration-time profiles were simulated, and the $I_{in,max}$ was estimated from the ratio of maximum blood concentration at the inlet and the blood-to-plasma ratio (34). PBPK model predicted inhibitor

Table I Summary of Input Parameters for Pravastatin, Cyclosporine, Gemfibrozil and Rifampin Used in the Simcyp Models

Parameters	Pravastatin	Source	Cyclosporine	Source	Gemfibrozil	Source	Rifampin[a]
Physicochemical properties							
Molecular weight (g/mol)	424.5	ACD	1202.6	ACD	250.3	ACD	823
log P/Log $D_{7.4}$	2.9/−0.9	ACD; (16)	2.8	ACD	4.3	ACD	3.28
Compound type	Monoprotic acid		Neutral		Monoprotic acid		Ampholyte
pK_a	4.6	ACD	–		4.75	ACD	1.7 and 7.9
Fraction unbound	0.47	(23,67)	0.068	(68)	0.03	(69)	0.15
Blood/plasma ratio	0.56	(23,67)	1.36	(70)	0.825	(69)	0.90
Absorption							
Absorption type	First-order		First-order		First-order		First-order
Fraction absorbed	0.47	(21)	0.86	(68)	1.0	(69)	1.0
Absorption rate constant (1/h)	1.25	(21)[b]	1.50	(49)[b]	3.0	(50,52)[b]	0.51
Caco-2 permeability ($\times 10^{-6}$ cm/s)	3.0	In-house data					
Distribution							
Distribution model	Whole-body PBPK (Rodgers *et al.*)		Whole-body PBPK (Polin and Theil)		Minimal PBPK		Minimal PBPK
Vss (L/kg)	–		–	(68,71)	0.13	(69)	0.33
Elimination							
Total Clearance (IV/PO) (L/h)	–		27.7 (IV)	(68,71)	7.12 (PO)	(69)	7.0 (IV)
Renal Clearance (L/h)	26.45	(21)					
Hepatobiliary transport							
Liver unbound fraction	0.51	(23)					
Passive diffusion (μL/min/10^{-6}cells)	0.5	SCHH					
$CL_{Int,uptake}$ (μL/min/10^{-6}cells)	1.9	SCHH					
Scaling factor (uptake)	31	Estimated[c]					
$CL_{Int,efflux}$ (μL/min/10^{-6}cells)	1.2	SCHH					
Scaling factor (efflux)	0.17	Estimated[c]					

ACD, Calculated using Advanced Chemistry Development (ACD/Labs) Software V11.02. (SciFinder 2007.1)

P, partition coefficient; pK_a, acid dissociation constant; V_{ss}, volume of distribution at steady state; IV, intravenous; PO, oral

[a] Rifampin input parameters were directly adopted from compound file "Sim-Rifampicin" of Simcyp compound library

[b] Estimated by compartment or non-compartment analysis of clinical oral pharmacokinetics data using WinNonlin version 5.2

[c] Estimated by fitting to intravenous pharmacokinetics data. See "Materials and Methods"

maximum portal vein concentrations were used for $I_{in,max}$. When only IC_{50} value was reported, it was converted into a Ki value assuming competitive inhibition (48).

RESULTS

In Vitro Hepatobiliary Transport

In vitro SCHH model was used to obtain the transport parameters for hepatobiliary disposition of pravastatin. Studies in the presence and absence of rifamycin SV or calcium yielded sinusoidal uptake, passive and efflux clearance values of 1.9, 0.5 and 1.2 μL/min/10^6cells, respectively (Table I). Hepatic uptake of pravastatin is majorly driven by active uptake mechanism, with about 4-fold higher active uptake clearance as compared to passive diffusion. Pravastatin also showed significant canalicular secretion in SCHH studies, suggesting the role of efflux transporters in the biliary excretion.

Pravastatin PBPK Model Development

The hepatic transport intrinsic clearance values along with the other input parameters, listed in Table I, were used to build the whole-body PBPK model for pravastatin. However, this initial model overpredicted the plasma time-concentration profile

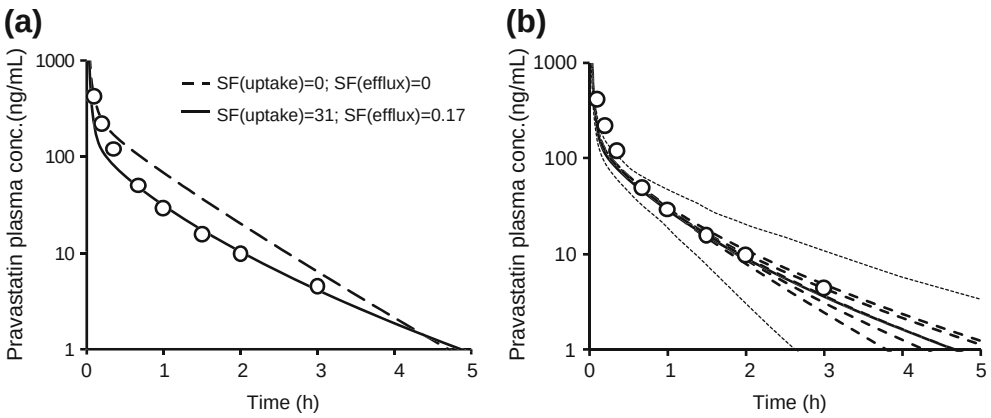

Fig. 1 Pravastatin plasma concentration-time profiles following intravenous administration of 9.9 mg dose. (**a**) Simulations of PBPK model without and with scaling factors for active hepatobiliary transport parameters. (**b**) Mean profile (*solid line*) of five trial simulations (*dashed lines*) and 95% confidence intervals (*dotted lines*) simulated using final model. Data points represent observed values taken from (21).

following intravenous dose (Fig. 1a). Model fitting to the intravenous data yielded scaling factors for the hepatic sinusoidal active uptake (SF_{uptake}) and canalicular efflux (SF_{efflux}) of about 31 and 0.17, respectively, while the rest of the input parameters remained as that of the initial model. Figure 1b shows the simulations of five trials of pravastatin following intravenous dosing, based on the final model. The predicted average intravenous clearance and the steady-state volume of distribution were within 30% of the observed values.

Pravastatin Oral Pharmacokinetics and Sensitivity Analysis

The final model best described the oral pravastatin plasma concentration-time profiles. Figure 2 shows log-normal plots of simulated and observed oral pharmacokinetics at four different dose levels obtained from previously reported separate clinical studies (21,28–31). The predictions are in agreement with clinical observation, and confirm the validity of the final model. Predicted mean AUC and Cmax values are within 20% of the observed values (Table II).

Parameter sensitivity analysis was performed to assess the influence of input parameters, including hepatic uptake and efflux intrinsic clearances, and passive diffusion across the sinusoidal membrane on the pravastatin systemic exposure (Fig. 3). Notably, hepatic uptake intrinsic clearance showed a predominant effect, with about 4-fold higher AUC and Cmax when the uptake clearance was lowered by an order of magnitude. However, AUC was sensitive to the hepatic efflux intrinsic clearance, while its effect on the Cmax was only minimal. In contrary, increase in passive diffusion resulted in increase of both the PK parameters.

DDI Predictions with PBPK Model

Cyclosporine and gemfibrozil models were developed using the input parameters listed in Table I. The predicted and observed plasma or blood time-concentration profiles for both cyclosporine and gemfibrozil suggest that the systemic exposure of both the perpetrator drugs was reasonably well predicted by the current models (Fig. 4). Similarly, simulation of rifampin model was comparable to the clinically observed plasma profile. While, the mean observed concentration-time profiles of these drugs are reasonably consistent in separate clinical studies (49–52), predicted and observed Cmax and AUC are within 20% error (Table II).

A wide range of *in vitro* Ki values for OATP1B1 inhibition are reported for cyclosporine (0.014-1.0 μM (34–38)), gemfibrozil (2.5–35.8 μM (36,40–43)) and rifampin (0.41–3.1 μM (36,37,44–46)). With the reported geometric mean *in vitro* Ki values of cyclosporine (0.17 μM) and gemfibrozil (11 μM), the PBPK model prediction of AUC change was only about 2-fold and 1.2-fold, respectively, suggesting some discrepancy between *in vitro* and *in vivo* inhibition potency (Fig. 5). Therefore, sensitivity analysis of *in vitro* Ki was performed to estimate the *in vivo* Ki, where the predicted magnitude of DDI is similar to that observed in clinical studies (53). With cyclosporine, the predicted AUC change using the most potent reported Ki (0.014 μM (34)) was lower than observed in separate clinical studies (28,31). Interestingly, no further change in AUC ratio was noted when the Ki of cyclosporine was further lowered (Fig. 5a); presumably due to complete inhibition of hepatic active uptake process.

At 600 mg twice daily dose, cyclosporine, with OATP1B1 and MRP2 inhibition potency (Ki) values of 0.014 μM (34) and 1.35 μM (39), respectively, increased plasma exposure of pravastatin (10 mg dose) as compared with control (Fig. 6a). However, the predicted increment in the AUC was only 4.4-fold, in comparison to about 10-fold change noted in the clinical studies (28,31). In case of gemfibrozil DDI simulations, OATP1B1 Ki of 2.5 μM (42) and 600 mg twice daily dose resulted in increased AUC and Cmax of pravastatin (40 mg dose) to an extent (1.94-fold)

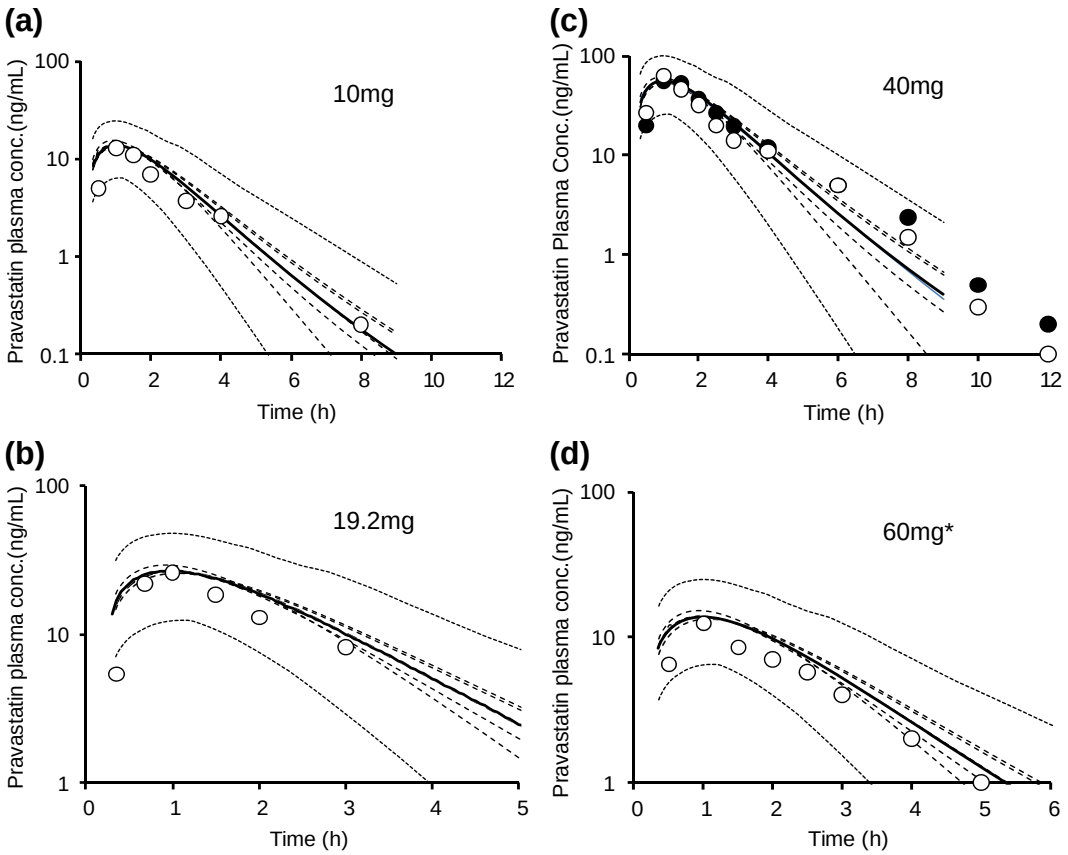

Fig. 2 Pravastatin plasma concentration-time profiles following oral administration of (**a**) 10 mg, (**b**) 19.2 mg, (**c**) 40 mg and (**d**) 60 mg dose. Mean profile (solid line) of five trial simulations (dashed lines) and 95% confidence intervals (dotted lines). Data points are observed mean values taken from a, 10 mg dose (28); b, 19.2 mg dose (21); c, 40 mg (29,30); d, 60 mg (31). *Profiles of 60 mg dose were normalized to 10 mg, as represented in the original report. Open and closed points represent data from separate studies.

similar to that observed in the clinic (2.02-fold (29)). Although, the observed and predicted plasma time-concentration profiles were reasonably similar up to 4 h post dosing, the current model underpredicted the plasma exposure at the later time points (Fig. 6b).

On the other hand, using the geometric mean *in vitro* Ki (0.93 μM), PBPK model reasonably predicted the AUC change with rifampin (Fig. 5c). Furthermore, in the lower range of *in vitro* Ki (0.41–0.7 μM), exposure change was well predicted by the PBPK model. The clinical pravastatin-rifampin DDI study with known exposure increase was reported in healthy Chinese volunteers (54); and interestingly, the pravastatin plasma exposure is relatively high (>4-fold) in the Chinese control group compared to Caucasian subjects at a similar dose (21). Due to the apparent ethnic differences in the pravastatin pharmacokinetics, the simulated concentration-time profile did not match with the observed profiles (not shown).

DDI Predictions Using Static (R-value) Model

The R-value for the corresponding *in vitro* Ki values were calculated, using the inhibitor free inlet maximum concentration ($fu.I_{in,max}$), to assess the predictability of DDI and to

Table II Observed and Predicted Pharmacokinetic Parameters of Pravastatin Following Oral Dosing

Pravastatin oral dose	Mean AUC (ng/mL.h)			Mean Cmax (ng/mL)		
	Observed	Predicted	PPE(%)*	Observed	Predicted	PPE(%)*
10 mg[a]	26.6	31.7	19	15.7	12.9	18
19.2 mg[b]	66.2	72.8	10	27.4	27.2	1
40 mg[c]	140.5	143.4	2	65.7	56.7	14
60 mg[⊥,d]	26.2	31.7	21	13.7	12.9	6

[a](28); [b](21); [c](29,30); [d](31).
[⊥]Dose normalized to 10 mg as provided in the original report.
*Percentage prediction error = 100x|(predicted-observed)/observed|

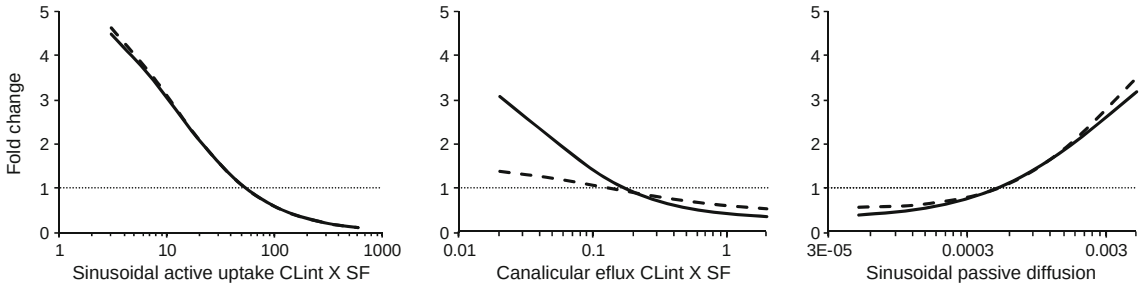

Fig. 3 Sensitivity analysis of hepatobiliary transport parameters on the oral pharmacokinetics of pravastatin. Simulated fold change from baseline in the AUC (solid line) and Cmax (dash line) of pravastatin, following 10 mg oral dose, as a function of hepatic active uptake, canalicular efflux and sinusoidal passive diffusion.

compare with the mechanistic PBPK model predictions. $I_{in,max}$ was obtained from PBPK model predicted inhibitor portal vein concentration profiles (Table III). In general, the R-values were relatively higher than the PBPK model predicted AUC ratios (Fig. 5). With cyclosporine *in vivo* Ki of 0.014 μM, which is used in current PBPK modeling, the R-value overpredicted the DDI magnitude. However, within the *in vitro* Ki range (0.014–1.0 μM), R-value varied between ~30 and 1.5. Similarly, R-value using gemfibrozil Ki of 2.5 μM indicated about 2.7-fold exposure change; while the range of *in vitro* Ki (2.5–11.2 μM) values yielded R-value between 2.7 and 1.4 (Fig. 5b). Notably, with geometric mean *in vitro* Ki value of cyclosporine (0.17 μM (34–38)) and gemfibrozil (11 μM (36,40–43)), the pravastatin exposure change was significantly underpredicted by the mechanistic PBPK and the static models. However, rifampin mean Ki (0.93 μM (36,37,44–46)) resulted in overprediction of DDI magnitude (Fig. 5c).

DISCUSSION

To establish a PBPK approach for pharmacokinetics and DDI predictions of drugs with hepatic transporter-mediated disposition, we used pravastatin as a model drug. The role of drug transporters in pravastatin disposition is underscored by the fact that pravastatin is significantly eliminated in bile (16,21,55). The hepatic sinusoidal uptake transporter, OATP1B1, and the canalicular efflux transporter, MPR2, are the major transporters involved in the hepatobiliary disposition of pravastatin in humans (16). In this study, we characterized the hepatobiliary transport using SCHH model and developed a whole-body PBPK model to describe the human oral pharmacokinetics and predict the DDIs, thought to be associated with the transporter-mediated hepatobiliary disposition.

Based on the intrinsic transport parameters obtained using SCHH studies, active sinusoidal uptake and canalicular efflux, inhibitable by rifamycin SV, appears to be the predominant processes determining the hepatobiliary disposition of pravastatin in humans. Furthermore, the passive diffusion across the sinusoidal membrane is lower than the canalicular efflux intrinsic clearance, suggesting that the pravastatin overall hepatobiliary transport is uptake rate-limited (56). Therefore, permeability-limiting model was used to capture the hepatobiliary disposition of pravastatin.

PBPK model directly using these *in vitro* transport parameters resulted in overprediction of pravastatin plasma concentrations, suggesting differences between *in vitro* and *in vivo* transport kinetics. Therefore, empirical scaling factors for the intrinsic clearances of active uptake (SF_{uptake}=31) and the canalicular efflux (SF_{efflux}=0.17), estimated based on fitting to human intravenous pharmacokinetics, were incorporated in the PBPK model (Fig. 1). Previous PBPK approaches incorporating five-compartment liver dispersion model also suggest the need for empirical scaling factors for hepatobiliary transport rates to predict human plasma concentration-time profiles of several OATP substrates, including pravastatin (22,23).

The apparent discrepancy in the *in vitro* - *in vivo* extrapolation of active transport kinetics, and the compulsion for scaling factors, could be due to (1) differences in transporter abundance in the *in vitro* (SCHH) experimental and the *in vivo* systems, as exemplified by about 5-fold up-regulation of MRP2 protein in SCHH (26); (2) possible functional activity differences between the two systems; and (3) potential active uptake of pravastatin into other tissues, which was not considered in the current model. For example, it is believed that OATP2B1 mediate uptake of statins into skeletal muscles (57), and may contribute to the drug distribution. With the current modelling approach, several possible combinations of sinusoidal passive diffusion and active transport rates may recover the pravastatin pharmacokinetic parameters observed in the clinic (22). However, passive diffusion is generally believed to be scaled accurately from *in vitro* to *in vivo*, presumably due to the lack of dependence on processes that could be influenced by culturing. Enterohepatic circulation may possibly influence the systemic exposure of pravastatin; however, the current model did not capture the processes due to the lack of definitive information on the input parameters (eg. % reabsorbed). Furthermore, a larger SF_{uptake} is required to recover the plasma-time profiles of pravastatin when enetrohepatic recirculation is considered. Overall, further understanding in these

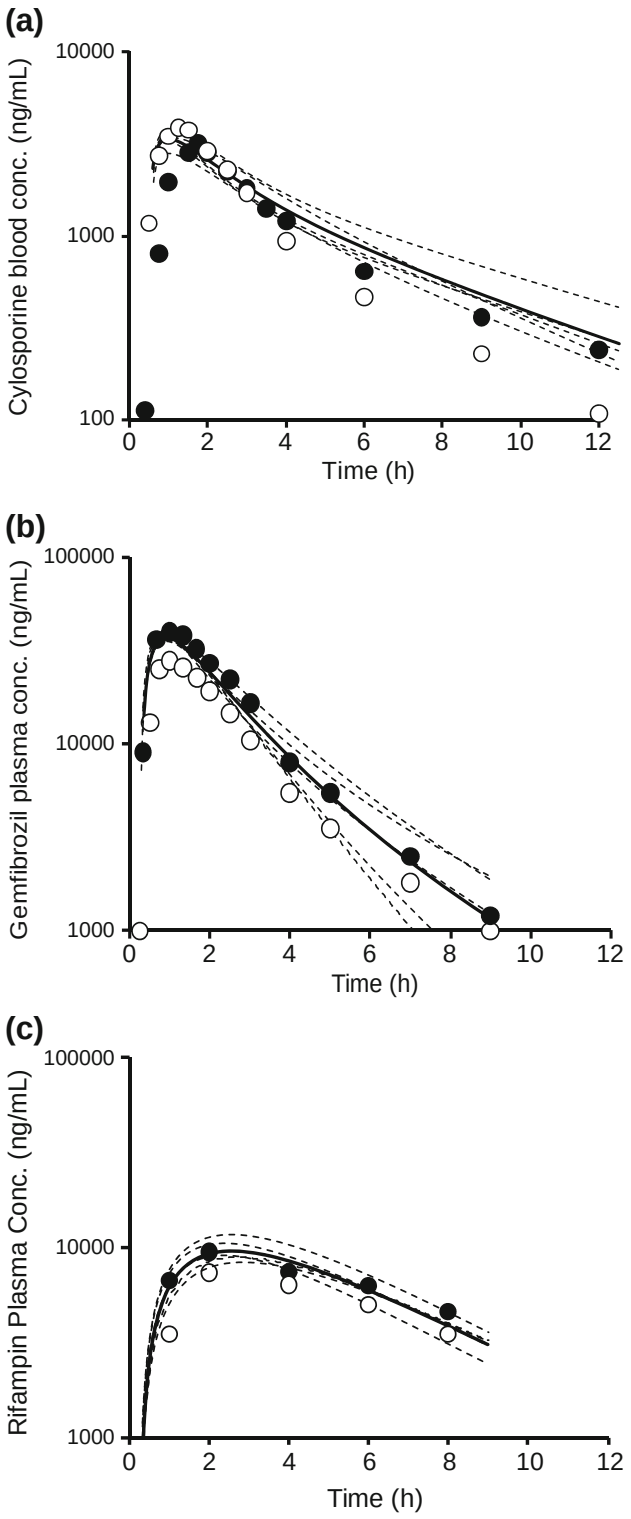

Fig. 4 (**a**) Cyclosporine blood concentration-time profiles, (**b**) Gemfibrozil plasma concentration-time profiles and (**c**) Rifampin plasma concentration-time profiles, following oral administration of 600 mg dose. Mean profile (solid line) of five trials (dashed lines) were simulated using models build. Mean observed values were taken from separate studies and normalized to 600 mg dose, assuming linear pharmacokinetics (49–52,66). Open and closed points represent data from separate studies.

areas is needed to justify the scaling factors and further validate or refine the current model. Nonetheless, the current PBPK model adequately described the mean pravastatin plasma concentration-time profiles following oral administration, within 20% error, at different dose levels (Fig. 2; Table II).

We examined the sensitivity of systemic exposure to the changes in hepatic uptake and efflux intrinsic clearances and the sinusoidal passive diffusion (Fig. 3). Simulations indicated that the systemic Cmax and AUC are most sensitive to changes in hepatic uptake kinetics, suggesting significant contribution of uptake transporters to the distribution and clearance of pravastatin. However, changes in efflux transport clearance has a minor effect on the systemic Cmax, while the systemic AUC seems to be influenced; although to a lesser degree than that noted with the change in uptake clearance. This relatively less sensitivity on systemic Cmax indicate minimal role of biliary efflux transport on the initial distribution. In contrary, increase in passive diffusion across the sinusoidal membrane increased both AUC and Cmax. Collectively, the significant effect of active uptake and passive diffusion suggest that transport across sinusoidal membrane is rate-limiting for pravastatin disposition (16,36).

Multiple drug therapy increases the risk of DDI. For example, patients with an organ transplant taking statins and cyclosporine are at increased risk for rhabdomyolysis, due to altered systemic and tissue exposure of statins (58). Gemfibrozil and rifampin also markedly raised the plasma concentrations of several OATP1B1 substrate drugs, such as atorvastatin, cerivastatin, lovastatin, pravastatin, rosuvastatin, repaglinide and simvastatin acid (59). Although inhibition of CYP3A4, CYP2C8 and transporters other than OATPs may explain some interactions with cyclosporine and gemfibrozil, it is now beyond doubt that inhibition of OATPs-mediated hepatic uptake, at least in part, contributes to the clinically observed DDIs (59). In order to predict the DDIs, it is important to build pharmacokinetic models for the perpetrator drugs that are co-dosed (3,7). Here, we established models for cyclosporine, gemfibrozil and rifampin, which adequately described their plasma concentration-time profiles following oral dosing (Fig. 4, Table III).

The average magnitude of interaction between pravastatin and cyclosporine was underpredicted, although most potent value (0.014 μM (34)) for OATP1B1 inhibition was used for modelling the DDI. Furthermore, at geometric mean (0.17 μM) of the reported *in vitro* Ki, the AUC ratio predicted by PBPK modelling was only about 2-fold. The underprediction may suggest that cyclosporine is a more potent inhibitor *in vivo* than *in vitro*. However, further decrease in the cyclosporine Ki (below 0.014 μM) did not recover the AUC ratio observed in the clinic (Fig. 5a). One plausible explanation for the DDI underprediction is the potential inhibition of the intestinal MRP2-mediated efflux by cyclosporine, leading to increased

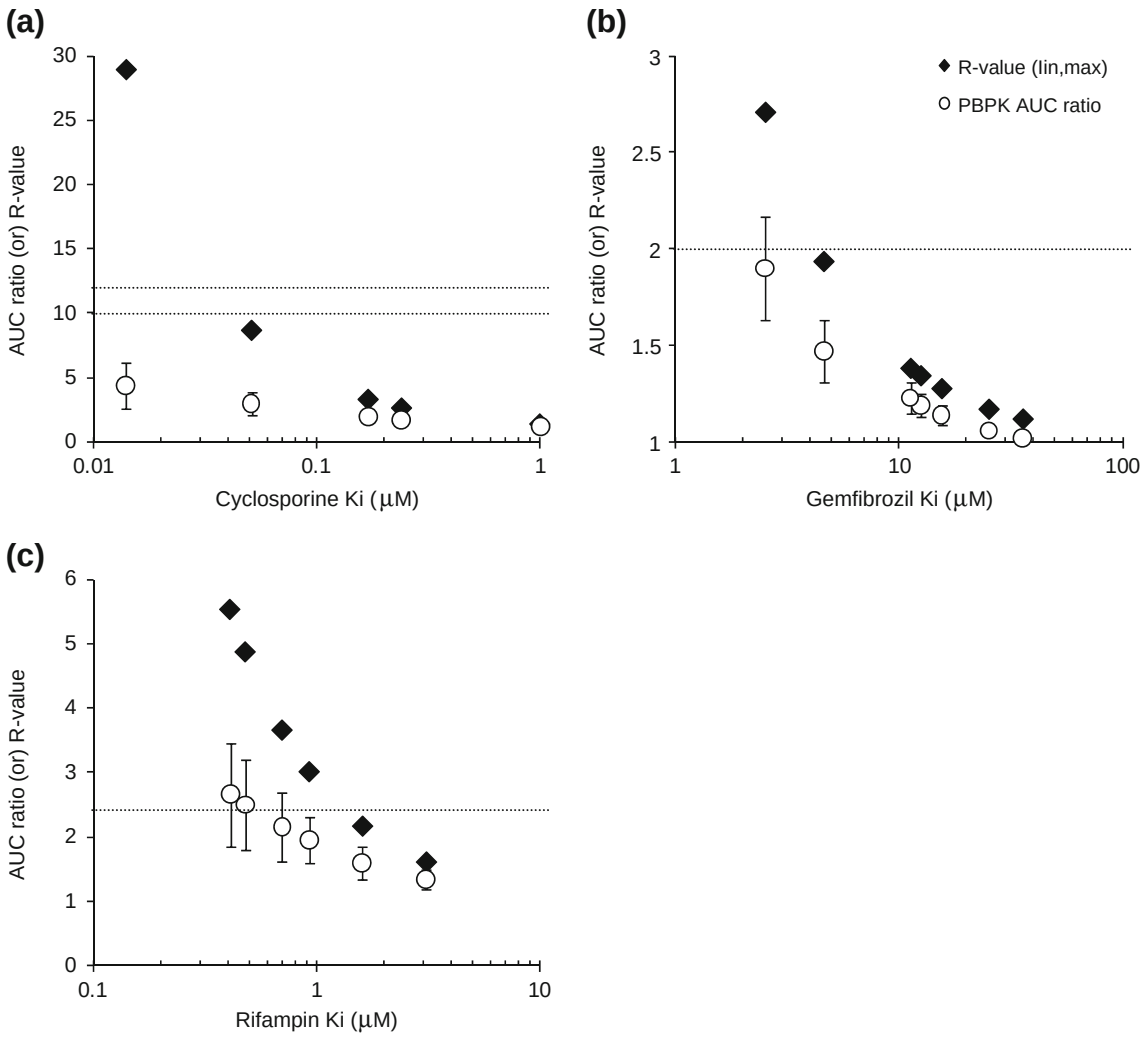

Fig. 5 Sensitivity analysis of cyclosporine, gemfibrozil and rifampin inhibition constant on the magnitude of drug-drug interaction of pravastatin, by PBPK and static models. (**a**) Predicted pravastatin-cyclosporine DDI magnitude at various reported *in vitro* Ki values (34–38). (**b**) Predicted pravastatin-gemfibrozil DDI magnitude at various reported *in vitro* Ki values (36,40–43). (**c**) Predicted pravastatin-rifampin DDI magnitude at various reported *in vitro* Ki values (36,37,44–46). Mean ± SD of AUC ratio was obtained by PBPK model simulations and R-values were calculated based on Eq. 1. Horizontal dotted lines represent mean observed AUC ratio in clinical studies (28,29,31,54).

oral exposure of pravastatin. Alternatively, cyclosporine may have reduced pravastatin renal clearance, which accounts for almost 50% of its total systemic clearance. However, no *in vitro* evidence of renal secretory transport inhibition or clinical evidence of renal clearance reduction of pravastatin, by cyclosporine, was reported. Pharmacogenomic studies demonstrated that increased expression or activity in *ABCC2* (MRP2) could lead to about 70% decrease in pravastatin oral bioavailability, suggesting the role of MPR2 in the intestinal absorption of pravastatin (60). Analogously, the *ABCG2* (BCRP) polymorphism significantly affected the pharmacokinetics of atorvastatin and rosuvastatin, presumably due to altered intestinal BCRP efflux activity (61). Although speculative, a possible 2-fold increase in Fa due to intestinal MRP2 inhibition by cyclosporine (IC50 2.7 μM (39)), could bridge the differences between the PBPK model predicted and the clinically observed AUC ratios (Fig. 7).

The significant contribution of increased intestinal absorption to the observed pravastatin-cyclosporine DDI is further substantiated by the clinical pharmacokinetic pattern of the changes in pravastatin Cmax and AUC (increase), but no change in the elimination half-life (28,31). As depicted with the simulated profiles (Fig. 6a), inhibition of only hepatobiliary transport by cyclosporine not only increases Cmax and AUC, but also considerably shorten the half-life, due to reduced volume of distribution. While cyclosporine inhibits a wide variety of efflux transporters along with MRP2, at the clinically relevant concentrations (39), the current PBPK model only captured MRP2-mediated hepatic efflux but not the intestinal efflux. In addition, it is believed that OATP2B1-

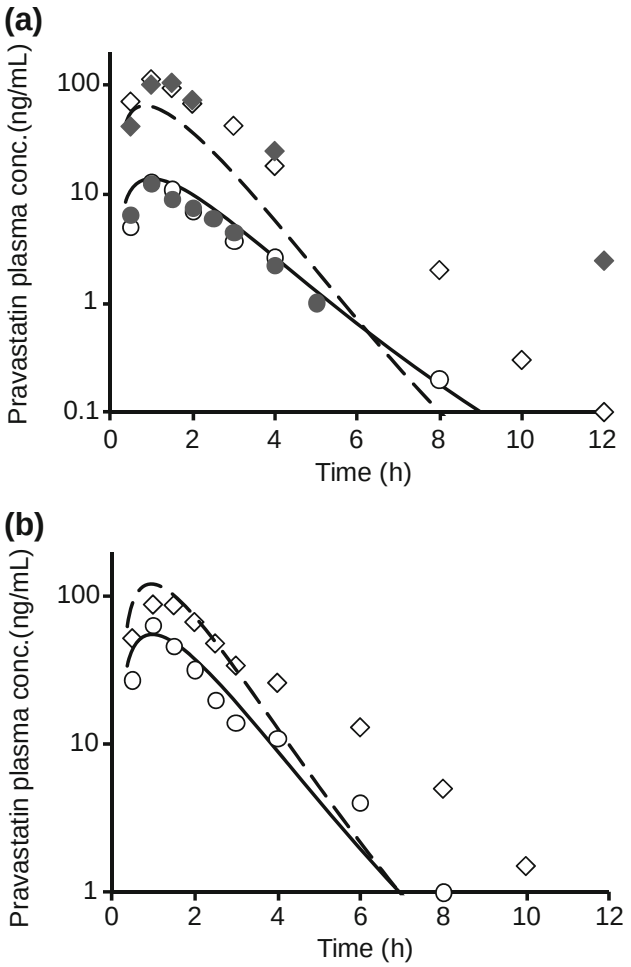

Fig. 6 Simulation of pravastatin drug-drug interaction with cyclosporine and gemfibrozil 600 mg dose. Pravastatin oral mean plasma time-concentration curves when dosed alone or in combination with (**a**) cyclosporine 600 mg and with (**b**) gemfibrozil 600 mg. The Ki of cyclosporine and gemfibrozil for OATP1B1 inhibition used for simulations were 0.014 μM and 2.5 μM, respectively. Data points represent mean observed plasma time-concentration profiles of pravastatin when dosed alone (circles) and in the presence of perpetrator (diamonds). Observed data were taken from (28,29,31). Open and closed points represent data from separate studies.

mediated uptake is responsible for the intestinal absorption of several statins, including pravastatin (62). Potential inhibition of both OATP2B1 and MRP2 by cyclosporine may cause differential absorption kinetics, and obscure the DDI findings. Additional mechanistic studies using specific transporter inhibitors are required to delineate the contribution of intestine and liver transporters to pravastatin disposition, in order to improve the DDI predictions. Alternatively, intravenous dosing of cyclosporine in DDI studies may result in interactions associated only with liver transporters, and thus can provide quantitative information on the functional involvement of intestine and liver. Eventually, complex models will be required to integrate these additional transporter kinetics in the intestine. Overall, our PBPK modelling suggest that the clinically observed magnitude of pravastatin-cyclosporine interaction is only partially associated with the inhibition of OATP1B1.

The average magnitude of interaction between pravastatin and gemfibrozil was well predicted, with the observed and predicted Cmax and AUC values within 20%, suggesting *in vivo* Ki of 2.5 μM for OATP1B1 inhibition by gemfibrozil. However, mean plasma concentrations at the later time points were underpredicted by the PBPK model, especially in the gemfibrozil treatment cohort. Similar to observed pravastatin-cyclosporine DDI, the half-life of pravastatin did not change in healthy volunteers co-dosed with gemfibrozil (29), suggesting contribution of non-OATP1B1 disposition processes, at least in part, to the pravastatin-gemfibrozil DDI. Notably, renal clearance of pravastatin was found to be reduced by about 40% when dosed with gemfibrozil (29). While, pravastatin is thought to be renally secreted via OAT3, gemfibrozil and its major metabolite gemfibrozil-1-O-β-glucuronide inhibit OAT3-mediated pravastatin transport *in vitro* with inhibition potency in the clinically relevant concentration range (63). Gemfibrozil-1-O-β-glucuronide also inhibit OATP1B1 (41) and therefore, persistent inhibition of OATP1B1, as well as OAT3, by the metabolite may account partially for the DDI. Extrapolation of the metabolite exposures and incorporation of complex model components for renal secretion may be needed to recover the later part of the plasma concentration-time profile. Nevertheless, the current PBPK model provided good quantitative predictions of the pravastatin-gemfibrozil DDI.

Table III Observed and Predicted Pharmacokinetic Parameters of Cyclosporine, Gemfibrozil and Rifampin Following Oral Dosing

Inhibitor (oral dose)	Mean AUC (ng/mL.h)			Mean Cmax (ng/mL)			$I_{in,max}$ (μM) $^{\Delta}$
	Observed	Predicted	PPE(%)*	Observed	Predicted	PPE(%)*	
Cyclosporine (600 mg) $^{\perp,a}$	11874$^{\perp}$	13593	14	3885$^{\perp}$	3463	11	7.8
Gemfibrozil (600 mg)^{b}	105000	99234	5	39500	37249	6	148.1
Rifampin (600 mg)^{c}	52260	57405	10	10390	9694	7	12.4

^{a} (49,51); ^{b} (52); ^{c} (66). $^{\perp}$ Dose normalized to 600 mg. *Percentage prediction error = 100x|(predicted-observed)/observed|

$^{\Delta}$ $I_{in,max}$, represent the PBPK model predicted inhibitor maximum portal vein concentration

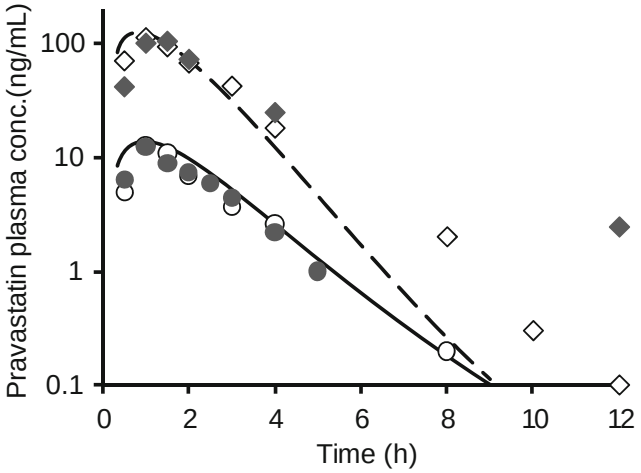

Fig. 7 Simulation of pravastatin drug-drug interaction with cyclosporine 600 mg dose, assuming a 2-fold increase in pravastatin Fa in the presence of cyclosporine. Pravastatin oral mean plasma time-concentration profiles when dosed alone (solid line) or in combination with cyclosporine 600 mg (dashed line). The Ki of cyclosporine for OATP1B1 inhibition used for simulations was 0.014 μM. Open and closed points represent mean observed plasma time-concentration profiles of pravastatin taken from Hedman *et al.* (28) and Park *et al.* (31).

A wide range of *in vitro* Ki values, for OATP1B1 inhibition, by cyclosporine (0.014-1.0 μM) and gemfibrozil (2.5–35.8 μM) are reported (34–38,40–43). Based on the sensitivity analysis, we estimated the *in vivo* Ki for the cyclosporine and gemfibrozil, because prediction of AUC changes using mean *in vitro* Ki values resulted in underprediction of DDIs with both the PBPK and static models. The current PBPK model suggested the *in vivo* Ki of cyclosporine, gemfibrozil and rifampin as 0.014 μM, 2.5 μM and 0.41–0.6 μM, respectively, which are essentially the most potent *in vitro* Ki values reported. Although, with cyclosporine the PBPK model underpredicted the pravastatin DDI, we note that this estimated *in vivo* Ki reasonably predicted DDI of other drugs with predominant hepatobiliary disposition (manuscript under preparation). The discrepancies between *in vitro* and *in vivo* Ki demand for careful considerations, not only for quantitative DDI assessment, but also to avoid false negative predictions.

Notably, reported geometric mean *in vitro* Ki values were about 12-fold and 4.5-fold greater than the estimated *in vivo* Ki for cyclosporine and gemfibrozil, respectively. This trend is consistent with the CYP-mediated DDIs, where relatively large differences were noted between the *in vitro* and *in vivo* Ki values for lipophilic inhibitors (cLogP >1) (53). The wide spread of reported *in vitro* Ki values and the disparity from the *in vivo* Ki might be due to different experimental conditions used and the extensive binding of these inhibitor drugs to the *in vitro* cell systems. The current PBPK approach may be used for estimating the *in vivo* Ki values for the inhibitors, when the clinical DDI data is available. However, challenges arise when attempting predictions for development candidate - to be tested as perpetrator. The unbound inhibition constant value ($Ki_{unbound}$ = *in vitro* Ki . fu_{inc}) provides an estimate of inhibition potency that is independent of non-specific binding to the *in vitro* system. Thus, the correction of the *in vitro* Ki for the fraction unbound in the incubations (fu_{inc}) may improve the DDI predictions. Apparent quantitative relationship between the microsomal or hepatocyte binding and the drug lipophilicity has been demonstrated (64,65), which may be useful to correct the *in vitro* Ki (53). It is likely that lipophilic drugs such as cyclosporine and gemfibrozil show fu_{inc} much smaller than unity in the cell-based experimental systems, resulting in a $Ki_{unbound}$ lower than the *in vitro* Ki. However, additional studies are necessary to evaluate if the *in vitro* Ki corrected for the fu_{inc} yield values similar to the *in vivo* Ki, estimated utilizing PBPK approach.

Prediction of transporter-mediated DDI based on static (R-value) model has been often used; and has been recommended by US FDA (7,14,47). Using the *in vivo* Ki values and $I_{in,max}$, we noted that the R-value predicted higher magnitude of DDI compared to the AUC ratio predicted by the PBPK modeling (Fig. 6). This is not surprising given the fact that static model only captures the maximum plasma concentration of the perpetrator, while the PBPK modeling accounts for temporal change in the perpetrator plasma concentration. Static model may be useful to avoid false negative predictions, but often yield false positive predictions. Overall, this study accentuates the need for adopting PBPK approaches over conventional methods for quantitative prediction of the transporter-mediated DDIs.

CONCLUSIONS

In conclusion, a PBPK model for predicting transporter-mediated disposition and DDIs of pravastatin was developed using *in vitro* transport kinetics and the scaling factors obtained by fitting to intravenous plasma concentration-time profile. While intravenous pharmacokinetic data was used in the current model to estimate transport scaling factors, we note that similar values for the scaling factors may also be obtained from the oral pharmacokinetic profiles (not shown). DDI prediction using *in vitro* Ki values for OATP1B1 inhibition resulted in misprediction with both the static and PBPK models, suggesting apparent discrepancies between *in vitro* and *in vivo* Ki. The use of *in vivo* Ki values and the current PBPK model yielded improved DDI predictions compared to the static model. Based on this study, we infer that inhibition of transporter-mediated hepatobiliary disposition do not completely explain the pravastatin AUC change observed with cyclosporine concomitant dosing. However, it is apparent that the DDIs with gemfibrozil and rifampin are predominantly associated with hepatic active uptake inhibition. While this study point towards certain limitations and knowledge gaps, the approach described can help establish reliable dynamic

models for pharmacokinetic and DDI predictions of drugs undergoing transporter-mediated hepatobiliary disposition.

ACKNOWLEDGMENTS & DISCLOSURES

The authors would like to thank Emi Kimoto and Yi-An Bi for conducting the SCHH studies, and Larry Tremaine and Dennis Scott for the valuable suggestions on the manuscript. All authors are full-time employees of Pfizer Inc.

REFERENCES

1. Boxenbaum H. Interspecies scaling, allometry, physiological time, and the ground plan of pharmacokinetics. J Pharmacokinet Biopharm. 1982;10(2):201–27.
2. Feng MR, Lou X, Brown RR, Hutchaleelaha A. Allometric pharmacokinetic scaling: towards the prediction of human oral pharmacokinetics. Pharm Res. 2000;17(4):410–8.
3. Huang SM, Rowland M. The role of physiologically based pharmacokinetic modeling in regulatory review. Clin Pharmacol Ther. 2012;91(3):542–9.
4. Rowland M, Peck C, Tucker G. Physiologically-based pharmacokinetics in drug development and regulatory science. Annu Rev Pharmacol Toxicol. 2011;51:45–73.
5. Ito K, Sugiyama Y. Use of clearance concepts and modeling techniques in the prediction of metabolic drug-drug interactions. Trends Pharmacol Sci. 2010;31(8):351–5.
6. Zhao P, Vieira Mde L, Grillo JA, Song P, Wu TC, Zheng JH, *et al.* Evaluation of exposure change of nonrenally eliminated drugs in patients with chronic kidney disease using physiologically based pharmacokinetic modeling and simulation. J Clin Pharmacol. 2012;52(1 Suppl):91S–108S.
7. USFDA. Drug interaction studies - study design, data analysis, implications for dosing, and labeling recommendations. Center for Drug Evaluation and Research (CDER). 2012.
8. De Buck SS, Mackie CE. Physiologically based approaches towards the prediction of pharmacokinetics: *in vitro-in vivo* extrapolation. Expert Opin Drug Metab Toxicol. 2007;3(6):865–78.
9. Jamei M, Marciniak S, Feng K, Barnett A, Tucker G, Rostami-Hodjegan A. The Simcyp population-based ADME simulator. Expert Opin Drug Metab Toxicol. 2009;5(2):211–23.
10. Jones HM, Gardner IB, Watson KJ. Modelling and PBPK simulation in drug discovery. AAPS J. 2009;11(1):155–66.
11. Varma MV, Gardner I, Steyn SJ, Nkansah P, Rotter CJ, Whitney-Pickett C, *et al.* pH-dependent solubility and permeability criteria for provisional biopharmaceutics classification (BCS and BDDCS) in early drug discovery. Mol Pharm. 2012;9(5):1199–212.
12. Wu CY, Benet LZ. Predicting drug disposition via application of BCS: transport/absorption/ elimination interplay and development of a biopharmaceutics drug disposition classification system. Pharm Res. 2005;22(1):11–23.
13. Fenner KS, Jones HM, Ullah M, Kempshall S, Dickins M, Lai Y, *et al.* The evolution of the OATP hepatic uptake transport protein family in DMPK sciences: from obscure liver transporters to key determinants of hepatobiliary clearance. Xenobiotica. 2012;42(1):28–45.
14. Giacomini KM, Huang SM, Tweedie DJ, Benet LZ, Brouwer KL, Chu X, *et al.* Membrane transporters in drug development. Nat Rev Drug Discov. 2010;9(3):215–36.
15. Kalliokoski A, Niemi M. Impact of OATP transporters on pharmacokinetics. Br J Pharmacol. 2009;158(3):693–705.
16. Shitara Y, Sugiyama Y. Pharmacokinetic and pharmacodynamic alterations of 3-hydroxy-3-methylglutaryl coenzyme A (HMG-CoA) reductase inhibitors: drug-drug interactions and interindividual differences in transporter and metabolic enzyme functions. Pharmacol Ther. 2006;112(1):71–105.
17. Akao H, Polisecki E, Kajinami K, Trompet S, Robertson M, Ford I, *et al.* Genetic variation at the SLCO1B1 gene locus and low density lipoprotein cholesterol lowering response to pravastatin in the elderly. Atherosclerosis. 2012;220(2):413–7.
18. Ieiri I, Higuchi S, Sugiyama Y. Genetic polymorphisms of uptake (OATP1B1, 1B3) and efflux (MRP2, BCRP) transporters: implications for inter-individual differences in the pharmacokinetics and pharmacodynamics of statins and other clinically relevant drugs. Expert Opin Drug Metab Toxicol. 2009;5(7):703–29.
19. Niemi M, Neuvonen PJ, Hofmann U, Backman JT, Schwab M, Lutjohann D, *et al.* Acute effects of pravastatin on cholesterol synthesis are associated with SLCO1B1 (encoding OATP1B1) haplotype *17. Pharmacogenet Genomics. 2005;15(5):303–9.
20. Nishizato Y, Ieiri I, Suzuki H, Kimura M, Kawabata K, Hirota T, *et al.* Polymorphisms of OATP-C (SLC21A6) and OAT3 (SLC22A8) genes: consequences for pravastatin pharmacokinetics. Clin Pharmacol Ther. 2003;73(6):554–65.
21. Singhvi SM, Pan HY, Morrison RA, Willard DA. Disposition of pravastatin sodium, a tissue-selective HMG-CoA reductase inhibitor, in healthy subjects. Br J Clin Pharmacol. 1990;29(2):239–43.
22. Jones HM, Barton HA, Lai Y, Bi YA, Kimoto E, Kempshall S, *et al.* Mechanistic pharmacokinetic modelling for the prediction of transporter-mediated disposition in human from sandwich culture human hepatocyte data. Drug Metab Dispos. 2012.
23. Watanabe T, Kusuhara H, Maeda K, Shitara Y, Sugiyama Y. Physiologically based pharmacokinetic modeling to predict transporter-mediated clearance and distribution of pravastatin in humans. J Pharmacol Exp Ther. 2009;328(2):652–62.
24. Ghibellini G, Leslie EM, Brouwer KL. Methods to evaluate biliary excretion of drugs in humans: an updated review. Mol Pharm. 2006;3(3):198–211.
25. Bi YA, Kazolias D, Duignan DB. Use of cryopreserved human hepatocytes in sandwich culture to measure hepatobiliary transport. Drug Metab Dispos. 2006;34(9):1658–65.
26. Li N, Singh P, Mandrell KM, Lai Y. Improved extrapolation of hepatobiliary clearance from *in vitro* sandwich cultured rat hepatocytes through absolute quantification of hepatobiliary transporters. Mol Pharm. 2010;7(3):630–41.
27. Liu X, LeCluyse EL, Brouwer KR, Lightfoot RM, Lee JI, Brouwer KL. Use of Ca2+ modulation to evaluate biliary excretion in sandwich-cultured rat hepatocytes. J Pharmacol Exp Ther. 1999;289(3):1592–9.
28. Hedman M, Neuvonen PJ, Neuvonen M, Holmberg C, Antikainen M. Pharmacokinetics and pharmacodynamics of pravastatin in pediatric and adolescent cardiac transplant recipients on a regimen of triple immunosuppression. Clin Pharmacol Ther. 2004;75(1):101–9.
29. Kyrklund C, Backman JT, Neuvonen M, Neuvonen PJ. Gemfibrozil increases plasma pravastatin concentrations and reduces pravastatin renal clearance. Clin Pharmacol Ther. 2003;73(6):538–44.
30. Kyrklund C, Backman JT, Neuvonen M, Neuvonen PJ. Effect of rifampicin on pravastatin pharmacokinetics in healthy subjects. Br J Clin Pharmacol. 2004;57(2):181–7.
31. Park JW, Siekmeier R, Merz M, Krell B, Harder S, Marz W, *et al.* Pharmacokinetics of pravastatin in heart-transplant patients taking cyclosporin A. Int J Clin Pharmacol Ther. 2002;40(10):439–50.
32. Rodgers T, Leahy D, Rowland M. Physiologically based pharmacokinetic modeling 1: predicting the tissue distribution of moderate-to-strong bases. J Pharm Sci. 2005;94(6):1259–76.
33. Rodgers T, Rowland M. Physiologically based pharmacokinetic modelling 2: predicting the tissue distribution of acids, very weak bases, neutrals and zwitterions. J Pharm Sci. 2006;95(6):1238–57.

34. Amundsen R, Christensen H, Zabihyan B, Asberg A. Cyclosporine A, but not tacrolimus, shows relevant inhibition of organic anion-transporting protein 1B1-mediated transport of atorvastatin. Drug Metab Dispos. 2010;38(9):1499–504.
35. Fehrenbach T, Cui Y, Faulstich H, Keppler D. Characterization of the transport of the bicyclic peptide phalloidin by human hepatic transport proteins. Naunyn Schmiedebergs Arch Pharmacol. 2003;368(5):415–20.
36. Hirano M, Maeda K, Shitara Y, Sugiyama Y. Drug-drug interaction between pitavastatin and various drugs via OATP1B1. Drug Metab Dispos. 2006;34(7):1229–36.
37. Konig J, Glaeser H, Keiser M, Mandery K, Klotz U, Fromm MF. Role of organic anion-transporting polypeptides for cellular mesalazine (5-aminosalicylic acid) uptake. Drug Metab Dispos. 2011;39 (6):1097–102.
38. Shitara Y, Itoh T, Sato H, Li AP, Sugiyama Y. Inhibition of transporter-mediated hepatic uptake as a mechanism for drug-drug interaction between cerivastatin and cyclosporin A. J Pharmacol Exp Ther. 2003;304(2):610–6.
39. Tang F, Horie K, Borchardt RT. Are MDCK cells transfected with the human MRP2 gene a good model of the human intestinal mucosa? Pharm Res. 2002;19(6):773–9.
40. Hinton LK, Galetin A, Houston JB. Multiple inhibition mechanisms and prediction of drug-drug interactions: status of metabolism and transporter models as exemplified by gemfibrozil-drug interactions. Pharm Res. 2008;25(5):1063–74.
41. Nakagomi-Hagihara R, Nakai D, Tokui T, Abe T, Ikeda T. Gemfibrozil and its glucuronide inhibit the hepatic uptake of pravastatin mediated by OATP1B1. Xenobiotica. 2007;37(5):474–86.
42. Schneck DW, Birmingham BK, Zalikowski JA, Mitchell PD, Wang Y, Martin PD, *et al.* The effect of gemfibrozil on the pharmacokinetics of rosuvastatin. Clin Pharmacol Ther. 2004;75(5):455–63.
43. Yamazaki M, Li B, Louie SW, Pudvah NT, Stocco R, Wong W, *et al.* Effects of fibrates on human organic anion-transporting polypeptide 1B1-, multidrug resistance protein 2- and P-glycoprotein-mediated transport. Xenobiotica. 2005;35(7):737–53.
44. Annaert P, Ye ZW, Stieger B, Augustijns P. Interaction of HIV protease inhibitors with OATP1B1, 1B3, and 2B1. Xenobiotica. 2010;40(3):163–76.
45. De Bruyn T, Fattah S, Stieger B, Augustijns P, Annaert P. Sodium fluorescein is a probe substrate for hepatic drug transport mediated by OATP1B1 and OATP1B3. J Pharm Sci. 2011;100(11):5018–30.
46. Lau YY, Huang Y, Frassetto L, Benet LZ. Effect of OATP1B transporter inhibition on the pharmacokinetics of atorvastatin in healthy volunteers. Clin Pharmacol Ther. 2007;81(2):194–204.
47. Karlgren M, Ahlin G, Bergstrom CA, Svensson R, Palm J, Artursson P. *In vitro* and *in silico* strategies to identify OATP1B1 inhibitors and predict clinical drug-drug interactions. Pharm Res. 2012;29 (2):411–26.
48. Brandt RB, Laux JE, Yates SW. Calculation of inhibitor Ki and inhibitor type from the concentration of inhibitor for 50% inhibition for Michaelis-Menten enzymes. Biochem Med Metab Biol. 1987;37 (3):344–9.
49. Bergman AJ, Burke J, Larson P, Johnson-Levonas AO, Reyderman L, Statkevich P, *et al.* Effects of ezetimibe on cyclosporine pharmacokinetics in healthy subjects. J Clin Pharmacol. 2006;46 (3):321–7.
50. Honkalammi J, Niemi M, Neuvonen PJ, Backman JT. Mechanism-based inactivation of CYP2C8 by gemfibrozil occurs rapidly in humans. Clin Pharmacol Ther. 2011;89(4):579–86.
51. Kajosaari LI, Niemi M, Neuvonen M, Laitila J, Neuvonen PJ, Backman JT. Cyclosporine markedly raises the plasma concentrations of repaglinide. Clin Pharmacol Ther. 2005;78 (4):388–99.
52. Tornio A, Niemi M, Neuvonen M, Laitila J, Kalliokoski A, Neuvonen PJ, *et al.* The effect of gemfibrozil on repaglinide pharmacokinetics persists for at least 12 h after the dose: evidence for mechanism-based inhibition of CYP2C8 *in vivo*. Clin Pharmacol Ther. 2008;84(3):403–11.
53. Kato M, Shitara Y, Sato H, Yoshisue K, Hirano M, Ikeda T, *et al.* The quantitative prediction of CYP-mediated drug interaction by physiologically based pharmacokinetic modeling. Pharm Res. 2008;25(8):1891–901.
54. Deng S, Chen XP, Cao D, Yin T, Dai ZY, Luo J, *et al.* Effects of a concomitant single oral dose of rifampicin on the pharmacokinetics of pravastatin in a two-phase, randomized, single-blind, placebo-controlled, crossover study in healthy Chinese male subjects. Clin Ther. 2009;31(6):1256–63.
55. Neuvonen PJ, Backman JT, Niemi M. Pharmacokinetic comparison of the potential over-the-counter statins simvastatin, lovastatin, fluvastatin and pravastatin. Clin Pharmacokinet. 2008;47(7):463–74.
56. Shitara Y, Horie T, Sugiyama Y. Transporters as a determinant of drug clearance and tissue distribution. Eur J Pharm Sci. 2006;27 (5):425–46.
57. Knauer MJ, Urquhart BL, Meyer zu Schwabedissen HE, Schwarz UI, Lemke CJ, Leake BF, *et al.* Human skeletal muscle drug transporters determine local exposure and toxicity of statins. Circ Res. 2010;106(2):297–306.
58. Omar MA, Wilson JP. FDA adverse event reports on statin-associated rhabdomyolysis. Ann Pharmacother. 2002;36(2):288–95.
59. Neuvonen PJ, Niemi M, Backman JT. Drug interactions with lipid-lowering drugs: mechanisms and clinical relevance. Clin Pharmacol Ther. 2006;80(6):565–81.
60. Niemi M, Arnold KA, Backman JT, Pasanen MK, Godtel-Armbrust U, Wojnowski L, *et al.* Association of genetic polymorphism in ABCC2 with hepatic multidrug resistance-associated protein 2 expression and pravastatin pharmacokinetics. Pharmacogenet Genomics. 2006;16(11):801–8.
61. Keskitalo JE, Zolk O, Fromm MF, Kurkinen KJ, Neuvonen PJ, Niemi M. ABCG2 polymorphism markedly affects the pharmacokinetics of atorvastatin and rosuvastatin. Clin Pharmacol Ther. 2009;86(2):197–203.
62. Varma MV, Rotter CJ, Chupka J, Whalen KM, Duignan DB, Feng B, *et al.* pH-sensitive interaction of HMG-CoA reductase inhibitors (statins) with organic anion transporting polypeptide 2B1. Mol Pharm. 2011;8(4):1303–13.
63. Watanabe T, Kusuhara H, Debori Y, Maeda K, Kondo T, Nakayama H, *et al.* Prediction of the overall renal tubular secretion and hepatic clearance of anionic drugs and a renal drug-drug interaction involving organic anion transporter 3 in humans by *in vitro* uptake experiments. Drug Metab Dispos. 2011;39(6):1031–8.
64. Austin RP, Barton P, Cockroft SL, Wenlock MC, Riley RJ. The influence of nonspecific microsomal binding on apparent intrinsic clearance, and its prediction from physicochemical properties. Drug Metab Dispos. 2002;30(12):1497–503.
65. Austin RP, Barton P, Mohmed S, Riley RJ. The binding of drugs to hepatocytes and its relationship to physicochemical properties. Drug Metab Dispos. 2005;33(3):419–25.
66. Panchagnula R, Kaur KJ, Singh I, Kaul CL. Bioequivalence of rifampicin when administered as a fixed-dose combined formulation of four drugs *versus* separate formulations. Methods Find Exp Clin Pharmacol. 2000;22(9):689–94.
67. Yamazaki M, Tokui T, Ishigami M, Sugiyama Y. Tissue-selective uptake of pravastatin in rats: contribution of a specific carrier-mediated uptake system. Biopharm Drug Dispos. 1996;17 (9):775–89.
68. Varma MV, Obach RS, Rotter C, Miller HR, Chang G, Steyn SJ, *et al.* Physicochemical space for optimum oral bioavailability: contribution of human intestinal absorption and first-pass elimination. J Med Chem. 2010;53(3):1098–108.

69. Todd PA, Ward A. Gemfibrozil. A review of its pharmacodynamic and pharmacokinetic properties, and therapeutic use in dyslipidaemia. Drugs. 1988;36(3):314–39.
70. Kurokawa N, Kadobayashi M, Yamamoto K, Arakawa Y, Sawada M, Takahara S, *et al*. *In-vivo* distribution and erythrocyte binding characteristics of cyclosporin in renal transplant patients. J Pharm Pharmacol. 1996;48(6):553–9.
71. Ptachcinski RJ, Venkataramanan R, Rosenthal JT, Burckart GJ, Taylor RJ, Hakala TR. Cyclosporine kinetics in renal transplantation. Clin Pharmacol Ther. 1985;38(3):296–300.